

# Adversarial Exposure Attack on Diabetic Retinopathy Imagery

Yupeng Cheng<sup>1</sup>, Felix Juefei-Xu<sup>2</sup>, Qing Guo<sup>1\*</sup>, Huazhu Fu<sup>3</sup>, Xiaofei Xie<sup>1</sup>,  
Shang-Wei Lin<sup>1</sup>, Weisi Lin<sup>1</sup>, Yang Liu<sup>1</sup>

<sup>1</sup> Nanyang Technological University, Singapore

<sup>2</sup> Alibaba Group, USA

<sup>3</sup> Inception Institute of Artificial Intelligence (IIAI), UAE

## Abstract

Diabetic retinopathy (DR) is a leading cause of vision loss in the world and numerous cutting-edge works have built powerful deep neural networks (DNNs) to automatically classify the DR cases via the retinal fundus images (RFIs). However, RFIs are usually affected by the widely existing camera exposure while the robustness of DNNs to the exposure are rarely explored. In this paper, we study this problem from the viewpoint of adversarial attack and identify a totally new task, *i.e.*, *adversarial exposure attack* generating adversarial images by tuning image exposure to mislead the DNNs with significantly high transferability. To this end, we first implement a straightforward method, *i.e.*, *multiplicative-perturbation-based exposure attack*, and reveal the big challenges of this new task. Then, to make the adversarial image naturalness, we propose the *adversarial bracketed exposure fusion* that regards the exposure attack as an element-wise bracketed exposure fusion problem in the Laplacian-pyramid space. Moreover, to realize high transferability, we further propose the *convolutional bracketed exposure fusion* where the element-wise multiplicative operation is extended to the convolution. We validate our method on the real public DR dataset with the advanced DNNs, *e.g.*, ResNet50, MobileNet, and EfficientNet, showing our method can achieve high image quality and success rate of the transfer attack. Our method reveals the potential threats to the DNN-based DR automated diagnosis and can definitely benefit the development of exposure-robust automated DR diagnosis method in the future.

## 1 Introduction

Diabetic retinopathy (DR) is the leading cause of vision impairment and blindness among working-age adults globally (Lee, Wong, and Sabanayagam 2015b). DR is an eye disease associated with diabetes and if DR can be detected in time, the progression to vision loss can be slowed or even averted. Currently, the DR detection is primarily a manual process that is time-consuming and requires trained clinicians to evaluate the digital retinal fundus images (RFIs). Time is the essence here because delayed results can lead to delayed treatment, or even lost follow-up communication. Therefore, the need for an automated DR detection and screening method has long been recognized.

DNN-based automated medical imagery recognition has become more popular nowadays, as an aid to human experts.

\*Qing Guo is the corresponding author: tsingqguo@gmail.com.

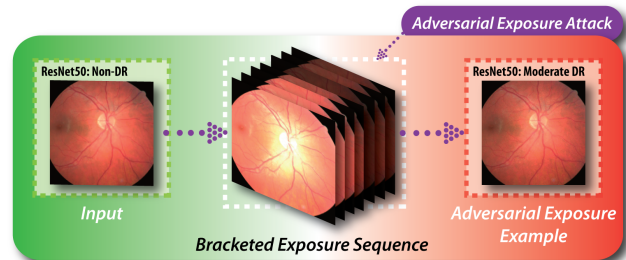


Figure 1: A normal retinal fundus image (left) is correctly classified as ‘non-DR’ by a pretrained ResNet50. After performing our adversarial exposure attack, the corresponding adversarial example is mis-predicted as ‘moderate DR’.

With the fast development of DNN-based image analysis and recognition techniques, we are allowing less human intervention and over time, the recognition system can become fully automated. DR detection based on retinal fundus image analysis is one such popular domain where automated DNN-based system is deployed (Gulshan et al. 2016; Mansour 2018; Gargeya and Leng 2017). For example, Kaggle built a DR detection competition and the DR is labeled as five levels: ‘0’ for no DR, ‘1’ for mild DR, ‘2’ for moderate DR, ‘3’ for severe DR, and ‘4’ for proliferative DR, which has draw great attention (Lee, Wong, and Sabanayagam 2015a).

With its apparent advantage of being efficient, the DNN-based DR detection does have some caveats, especially when faced with fundus images that exhibit various degradations. Low quality fundus images can lead to higher uncertainty in clinical observation and a risk of misdiagnosis. One major cause of low quality in retinal fundus images is uneven illumination or exposure. This is partly caused by the fact that the retina cannot be illuminated internally and both incident and reflected imaging beams have to traverse the pupil and partly by the spherical geometry of the eye that creates significant inter-reflection, resulting in shading artifacts (Shen et al. 2020).

In this work, we set out to reveal such a vulnerability for DNN-based DR detection by carefully tuning the image exposure to mislead the DNNs, and we name the new task: the adversarial exposure attack. We first implement a straightforward method, *i.e.*, *multiplicative-perturbation-based ex-*

posure attack, and reveal the big challenges of this new task. Then, to achieve high image quality, we propose the *adversarial bracketed exposure fusion* that regards the exposure attack as an element-wise bracketed exposure fusion problem in the Laplacian-pyramid space. Moreover, to realize high transferability, we further propose the *convolutional bracketed exposure fusion* where the multiplicative fusion is extended to the element-wise convolution. We have validated our method on a real public DR dataset with the powerful DNNs, *e.g.*, ResNet50, MobileNet, and EfficientNet, and shown that our method can not only achieve high image quality but high success rate of the transfer attack. In a larger sense, our method reveals the potential threats to the DNN-based DR automated diagnosis and can definitely benefit the development of exposure-robust automated DR diagnosis method in the future.

## 2 Related Work

### 2.1 Diabetic Retinopathy Grading

The traditional automatically DR grading methods are based on hand-crafted features. They utilized retinopathic manifestations including exudates, hemorrhages, hemes and microaneurysms as well as normal retina components such as blood vessels and optic discs. Silberman *et al.* (Silberman *et al.* 2010) extract SIFT features from input images. Afterwards, it trains a support vector machine (SVM) classifier to recognize the exudates in the retinal image and predicts different stages of DR depending on the result. Akram *et al.* (Akram *et al.* 2014) uses filter banks and a hybrid classifier, which is consist of m-Mediods based model and Gaussian mixture model, to realize lesion detection for grading of DR. Kumar *et al.* (Kumar *et al.* 2017) extends the multivariate generalized-Gaussian distribution to a reproducing kernel Hilbert space to generate a kernel generalized-Gaussian mixture model (KGGMM) for robust statistical learning.

In the past few years, many researchers address this problem with the help of deep neural network (DNN). Yang *et al.* (Yang *et al.* 2017) utilizes the annotations of location information, *e.g.*, microaneurysms *etc.*, to design a two-stage DNN network for joint lesion detection and DR grading. Gargeya *et al.* (Gargeya and Leng 2017) identify DR severity with a DNN classification model for diagnosing DR. Besides, some articles tried to explore and utilize the internal relationship between DR and diabetic macular edema (DME) to improve the performance in grading both diseases. Gulshan *et al.* (Gulshan *et al.* 2016) built a DNN model based on Inception-v3 architecture for grading DR and DME. After that, Krause *et al.* (Krause *et al.* 2018) outperformed it with Inception-v4 architecture. More recently, CANet (Li *et al.* 2019) integrates a disease-specific attention module as well as a disease-dependent attention module in a unit network to further improve the overall performance on grading DR and DME. Although achieving great progress, existing works do not consider the influence of a common phenomenon, *i.e.*, camera exposure, that is frequently happened in the diagnosis process.

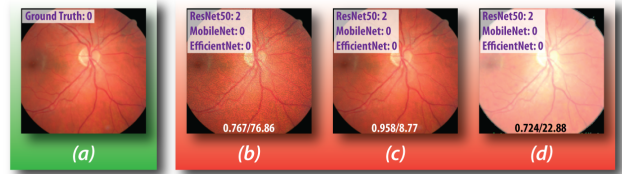


Figure 2: Recognition visualization results of an example input (a) and adversarial examples (b-d) generated by different realizations of our method in Sec. 3. (b) is produced by EQ. 1. (c) is produced by bracketed exposure fusion (BEF). (d) is produced by convolutional bracketed exposure fusion (CBEF). Ground truth label is listed on the top-left of input image. For each adversarial examples, the predictions of three models, *i.e.*, ResNet50, MobileNet, EfficientNet, are listed on the top-left. Two values on the bottom refer to their image quality assessment values, *i.e.*, SSIM and BRISQUE.

### 2.2 Adversarial Attack

Although DNN techniques facilitate the artificial intelligent in terms of many aspects, including image classification (He *et al.* 2016), detection (He *et al.* 2017), as well as the tasks in medical field. However, recent studies show that just tiny perturbation, called adversarial example, can totally mislead the prediction result of a well-trained DNN model (Szegedy *et al.* 2013). Generally, there are two kinds of adversarial attacks: whitebox attack and blackbox attack. In the setting of whitebox attack, the attack method can fully access the DNN model. Szegedy *et al.* (Szegedy *et al.* 2013) first address the generation of adversarial examples as a optimization problem. Goodfellow *et al.* then propose a one-stop method to efficiently produce adversarial examples named as fast gradient sign method (FGSM). Afterwards, Kurakin *et al.* (Kurakin, Goodfellow, and Bengio 2016) utilize iterative optimization to improve its performance. Before long, Dong *et al.* (Dong *et al.* 2018) further upgrade this method by applying the momentum term. Recently, Dong *et al.* (Dong *et al.* 2019) also explore how to enhance the transferability of adversarial examples. Other kinds of whitebox attacks, such as DeepFool (Moosavi-Dezfooli, Fawzi, and Frossard 2016), sacrifices the time complexity generating tiny perturbations in a simple way. Papernot *et al.* (Papernot *et al.* 2016) achieves the adversarial attack by restricting the  $\ell_0$  norm, which perturbs only a few pixels in the image. Su *et al.* (Su, Vargas, and Sakurai 2019) propose an attack method conducting adversarial attack with merely one pixel's modification. Carlini *et al.* (Carlini and Wagner 2017) produces extremely imperceptible perturbations by optimizing crafted object functions under different norms. Except the additive attacks, Guo *et al.* (Guo *et al.* 2020b) recently introduce a innovative way that attacks the input by blurring operation. Blackbox attack means that the attacker has no prior information of the target DNN model. In that case, Chen *et al.* (Chen *et al.* 2017) produce adversarial examples by estimating the gradients of the target model. Some works (Baluja and Fischer 2017; Hayes and Danezis 2017) train an attacker neural network to realize blackbox attack. Besides, Guo *et al.* (Guo *et al.* 2019) propose a simple way of constructing the adversarial perturbation in discrete cosine transform

(DCT) space and reach similar blackbox attack capability, yet, with less searching steps. More recently, Wang *et al.* (Wang et al. 2019) achieve blackbox attack through morphing way.

Note that, existing adversarial attacks mainly focus on the additive noise perturbation that could not be found in our daily life and could not help analyze the effects of real-world degradation, *e.g.*, camera exposure. In this work, we propose a totally novel exposure-based adversarial attack simulating the real bracketed exposure fusion in the photographer, which would help reveal the potential threats to DNN-based DR automated diagnosis.

### 3 Methodology

#### 3.1 Adversarial Exposure Attack on DR Imagery

Following the general camera exposure process, we can represent an exposure-degraded DR image ( $\mathbf{X}^e$ ) as the multiplication between a clean image  $\mathbf{X}$  and an exposure map  $\mathbf{E}$  having the same size with  $\mathbf{X}$ , *i.e.*,

$$\mathbf{X}^e = \mathbf{X} \odot \mathbf{E} \quad (1)$$

where  $\odot$  represents the element-wise multiplication. Like existing additive-perturbation-based adversarial attacks (Goodfellow, Shlens, and Szegedy 2014), we can naively realize a multiplicative-perturbation-based adversarial attack against a pre-trained DNN (*i.e.*,  $\phi(\cdot)$ ) by optimizing the following objective function

$$\arg \max_{\mathbf{E}} J(\phi(\mathbf{X} \odot \mathbf{E}), y), \text{ subject to } \|\mathbf{E} - 1\|_p < \epsilon \quad (2)$$

where  $J(\cdot)$  represents the image classification loss function, *i.e.*, the cross-entropy function, and  $y$  is the ground truth category of the  $\mathbf{X}$ .  $\epsilon$  controls the perturbation degree.

Although above method is simple and easy to implement, we argue that it cannot realize the desired exposure attack: ❶ camera exposure usually leads to spatial-smooth variation across the DR images. However, above method generates noise-like DR images (*e.g.*, Fig. 2 (b)) that are easily perceived and can be hardly regarded as the natural camera exposure factor, thus is less meaningful for the exposure-robustness analysis of DNNs. To address this problem, we propose the *adversarial bracketed exposure fusion* based attack in Sec. 3.2 that can generate local smooth variation with the Laplacian pyramid representation and adversarial tuned fusion weight maps. ❷ From the viewpoint of adversarial attack, above method can hardly achieve high transferability where the adversarial exposure example is generated from one DNN and used to attack another one. To alleviate this challenge, we further extend the multiplicative to the convolution perturbation with which we can realize high transferability with spatial-smooth intensity variation.

#### 3.2 Adversarial Bracketed Exposure Fusion (BEF)

To generate adversarial and spatial smooth exposure, we regard it as a bracketed exposure fusion problem (Mertens, Kautz, and Van Reeth 2009) where multi bracketed exposure images are first generated and fused within the Laplacian-pyramid space. The fusion weight maps for all images are tuned to let the image can fool DNNs.

**Bracketed exposure sequence generation.** Exposure bracketing is a well-known term in the photographer where one picture is taken at a given exposure, one or more brighter, and one or more darker, helping generate the most satisfactory image. Inspired by this technique, given a DR image  $\mathbf{X}$ , we generate an exposure sequence  $\{\mathbf{X}_i\}_{i=1}^N$  by

$$\mathbf{X}_i = \mathbf{X} \cdot 2^{e_i} \quad (3)$$

where  $e_i$  denotes the exposure shifting value and we set it in a range of  $[-\lambda, \lambda]$  with  $\lambda > 0$ . Intuitively, when we have  $e_i > 0$  the  $\mathbf{X}$  would be brighter otherwise darker.

**Bracketed exposure fusion.** To avoid generating noise-like patterns, we conduct fusion in the Laplacian-pyramid space. Similar solution has been adopted in image blending. Specifically, we decompose each bracketed exposure image, *e.g.*,  $\mathbf{X}_i$  to a Laplacian pyramid (LP) representation. The process is represented as  $\mathcal{L}(\mathbf{X}_i) = \{\hat{\mathbf{X}}_i^l\}_{l=1}^L$  where  $\hat{\mathbf{X}}_i^l$  denotes the  $l$ -th level decomposition of the  $\mathbf{X}_i$ . Moreover, for each  $\hat{\mathbf{X}}_i^l$ , we assign a weight map denoted as  $\mathbf{W}_i^l$  having the same size with  $\hat{\mathbf{X}}_i^l$ . Then, we can fuse the bracketed exposure images with their weight maps at each level

$$\hat{\mathbf{X}}^{e,l} = \sum_{i=1}^N \mathbf{W}_i^l \odot \hat{\mathbf{X}}_i^l, \text{ subject to } \sum_{i=1}^N \mathbf{W}_i^l = \mathbf{1}, \quad (4)$$

where the constraint term means the  $\{\mathbf{W}_i^l\}$  should be normalized at each level. Then, the fusion results of all levels, *i.e.*,  $\{\hat{\mathbf{X}}^{e,l}\}_{l=1}^L$ , are used to reconstruct the final result

$$\mathbf{X}^e = \mathcal{L}^{-1}(\{\hat{\mathbf{X}}^{e,l}\}_{l=1}^L) = \mathcal{L}^{-1}\left(\left\{\sum_{i=1}^N \mathbf{W}_i^l \odot \hat{\mathbf{X}}_i^l\right\}_{l=1}^L\right), \quad (5)$$

where  $\mathcal{L}^{-1}(\cdot)$  denotes the inverse LP decomposition. With Eq. 5, we can define the *adversarial bracketed exposure fusion* based attack, that is, we can tune all weight maps to let the final fused DR image fool DNNs

$$\arg \max_{\{\mathbf{W}_i^l\}} J\left(\phi\left(\mathcal{L}^{-1}\left(\left\{\sum_{i=1}^N \mathbf{W}_i^l \odot \hat{\mathbf{X}}_i^l\right\}_{l=1}^L\right)\right), y\right), \quad (6)$$

subject to  $\forall l, \sum_{i=1}^N \mathbf{W}_i^l = \mathbf{1}.$

As shown in Fig. 2, the proposed BEF attack can generate noiseless and naturalness adversarial examples. Nevertheless, according to our evaluation, such attack still cannot help achieve high transferability across different models. One possible reason is that the linear fusion via element-wise weight maps is hard to represent complex perturbation patterns that could fool DNNs.

#### 3.3 Convolutional Bracketed Exposure Fusion (CBEF)

To address the low transferability of the *adversarial bracketed exposure fusion* based attack, we extend the element-wise linear fusion to the convolutional way with more parameters can be tuned. Specifically, we represent Eq. 5, as

$$\mathbf{X}^e = \mathcal{L}^{-1}(\{\hat{\mathbf{X}}^{e,l}\}_{l=1}^L) = \mathcal{L}^{-1}\left(\left\{\sum_{i=1}^N \mathbf{K}_i^l \otimes \hat{\mathbf{X}}_i^l\right\}_{l=1}^L\right), \quad (7)$$

where  $\otimes$  denotes the element-wise convolution where each position of  $\hat{\mathbf{X}}_i^l$  has been processed by a corresponding kernel in  $\mathbf{K}_i^l$ . For example, if we have  $\hat{\mathbf{X}}_i^l \in \mathbb{R}^{H \times W}$ , the kernel should be  $\mathbf{K}_i^l \in \mathbb{R}^{H \times W \times K^2}$ , that is, the  $p$ -th element of  $\hat{\mathbf{X}}_{i,p}^l$  is proposed a kernel  $\mathbf{K}_{i,p}^l \in \mathbb{R}^{K \times K}$  that is the reshaped version of the  $p$ -th element of  $\mathbf{K}_i^l$ . We denote  $K$  as the kernel size. With Eq. 7, we can reformulate Eq. 6 as

$$\arg \max_{\{\mathbf{K}_i^l\}} J \left( \phi \left( \mathcal{L}^{-1} \left( \left\{ \sum_{i=1}^N \mathbf{K}_i^l \otimes \hat{\mathbf{X}}_i^l \right\}_{l=1}^L \right) \right), y \right), \quad (8)$$

subject to  $\forall l, \sum_{i=1}^N \sum_{p,q} \mathbf{K}_{i,p,q}^l = \mathbf{1}$ .

### 3.4 Optimization and Attack Algorithm

For each kernel, we use the sign gradient descent to optimize Eq. 6 and have

$$\mathbf{K}_{i,t}^l = \mathbf{K}_{i,t-1}^l + \alpha \text{sign}(\nabla_{\mathbf{K}_{i,t-1}^l} J), \quad (9)$$

where  $\text{sign}(\cdot)$  denotes the sign function and  $\alpha$  is the optimizing stepsize. The attacking process can be simply summarized as follows: *First*, we initialize the kernel  $\mathbf{K}$  as an identity version where  $\hat{\mathbf{X}}_i^l = \mathbf{K}_i^l \otimes \hat{\mathbf{X}}_i^l$ . *Second*, we calculate  $\mathbf{X}^e$  via Eq. 7. Then, we calculate the loss via  $J(\cdot)$  in Eq. 9 and perform back-propagation and update  $\mathbf{K}$  via Eq. 9. After that, we go back to the second step to further optimization till the maximum iteration number is reached.

## 4 Experiments

In this section, we demonstrate the attack capability as well as transferability of our method. We first describe the experimental setting in Sec. 4.1. Then, we report the comparison results with six additive-perturbation-based baseline methods in Sec. 4.2. Finally, we also explore the influence of each component on the transfer attack of our method in Sec. 4.3.

### 4.1 Setup

**Dataset.** In this part, we conduct our experiments on the EyePACS 2015 dataset (Lee, Wong, and Sabanayagam 2015a), which is one of the largest retinal image dataset and used in many recent DR related works (Gargeya and Leng 2017; Zhou et al. 2019). The DR is graded from 0-4 indicating the severities of patients<sup>1</sup>. To be specific, 0, 1, 2, 3, 4 refer to No DR, mild DR, moderate DR, severe DR and proliferative DR, respectively.

**Metrics.** We select the success rate for the evaluation of attack capability. Besides, our adversarial output should keep a satisfactory image quality for human vision system since a retinal fundus image with severe perturbation would be easily wiped off by doctors or operating staff. As a result, image quality assessment (IQA) is also introduced in our experiments. We choose structural similarity (SSIM) (Wang

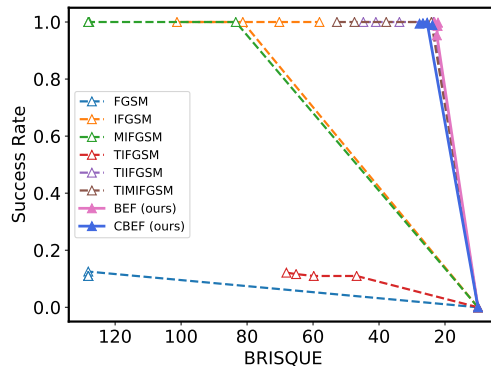
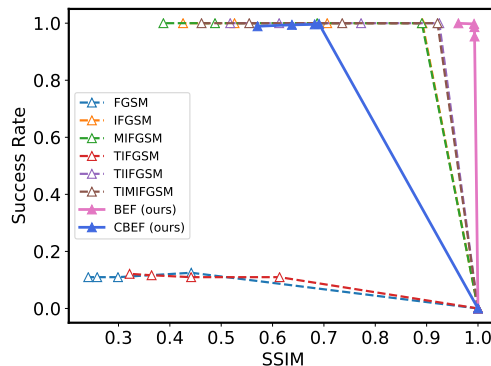


Figure 3: Attack success rate along with SSIM and BRISQUE for six baseline methods and our two attacks, *i.e.*, BEF and CBEF. Our curves are generated by tuning attack step size  $\alpha$  in Eq. 9 from 0.005 to 0.1. For the six additive-perturbation-based attacks, we tune the maximum perturbation ranges from 16 to 64 with the max intensity of 255.

et al. 2004) as our IQA metric for it considering the perceived change in structural information. Moreover, a non-reference IQA metric is also introduced in our experiments, *i.e.*, dubbed blind/referenceless image spatial quality evaluator (BRISQUE) (Mittal, Moorthy, and Bovik 2012), to further evaluate the naturalness of images for human beings. Overall, we select attack success rate, SSIM and BRISQUE for evaluating the performance of our method as well as all of the baselines.

**Models.** To evaluate the attack capability of our method against to different neural networks, we introduce three widely-used models including ResNet50 (He et al. 2016), MobileNet (Howard et al. 2017) and EfficientNet (Tan and Le 2019). They are all pre-trained on ImageNet dataset and fine-tuned on the EyePACS dataset, achieving top recognition accuracy.

**Baselines.** We choose six advanced additive-perturbation-based adversarial attacks as the baseline methods: fast gradient sign method (FGSM) (Goodfellow, Shlens, and Szegedy 2014), iterative fast gradient sign method (IFGSM) (Kurakin, Goodfellow, and Bengio 2016), momentum iterative fast gradient sign method (MIFGSM) (Dong et al. 2018),

<sup>1</sup>Detailed information about the dataset could be found in <https://www.kaggle.com/c/diabetic-retinopathy-detection>

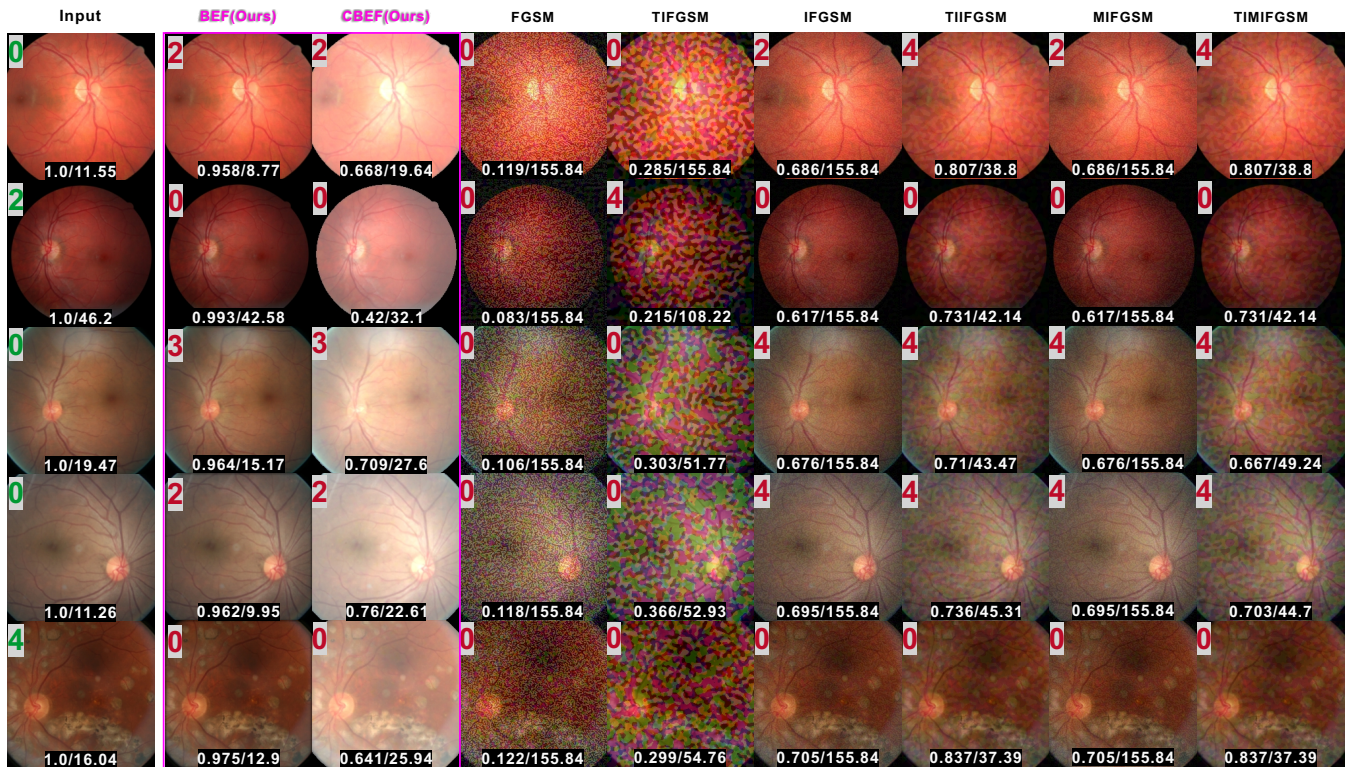


Figure 4: Visualization results of adversarial examples crafted for the ResNet50, using our methods, *i.e.*, BEF and CBEF, as well as six baseline attacks. For each image, its DR grading result through ResNet50 is displayed on the top-left. Two numbers at the bottom are SSIM, and BRISQUE values. The five inputs (1st column) are correctly classified to their ground truth DR grade, and the numbered label can be used to gauge the classification of all the remaining attack algorithms (column 2-8).

as well as their translation-invariant (TI) version proposed in (Dong et al. 2019) which are denoted as TIFGSM, TIIFGSM, and TIMIFGSM, respectively.

## 4.2 Comparison with Baseline Methods

**Quantitative Analysis.** We first demonstrate the attack capability of our method by evaluating the adversarial examples crafted for ResNet50. We should compare all methods based on the image quality of adversarial examples as well as the attack success rate for fair comparison. Therefore, we tune parameters for different attacks to generate multiple success rate-SSIM/BRISQUE curves for clear visualization comparison. To be concrete, we tune the maximum perturbation value of additive-perturbation-based attacks ranging from 16 to 64 and the step size of our attack methods (*i.e.*, BEF and CBEF), *i.e.*,  $\alpha$  in Eq. 9, from 0.005 to 0.1.

We show the comparison results in Fig. 3 and have the following observations: ❶ Most attacks achieve almost 100% attack success rate indicating that our methods and baselines have enough capability in attacking the target model. ❷ Although most attacks have a similar success rate of 100%, their image qualities are various. MIFGSM, TIMIFGSM and TIIFGSM outperform other baselines as well as our CBEF in terms of SSIM metric, while they are all beaten by our BEF. Specifically, TIMIFGSM has a best SSIM value of 0.95 among baselines, and the best SSIM value of our

CBEF is only 0.7. However, the lowest SSIM value of BEF is 0.97 which outperforms all attack methods with similar attack success rate. We mainly attribute the advantage of BEF to the Laplacian pyramid fusion process, which effectively depress the noise pattern. Compared with additive-perturbation-based attacks and BEF, our CBEF perturbs the input image by mutating each pixel through its neighbours in all exposure images, leading to higher transferability as well as weakness in SSIM metric. In contrast to the SSIM metric, our two attacks have a significant advantage when considering BRISQUE metric. Both methods have similar BRISQUE values around 20, surpassing all results of baselines. It proves that our attack methods show a perceptible change comparing with original image, but they still keep a satisfactory quality in terms of human vision system.

**Qualitative Analysis.** To illustrate the advantage of our method in detail, we visualize several examples in Figure. 4 and observe that BEF keeps the best image quality, and CBEF takes the second place in terms of BRISQUE. Specifically, the SSIM values of TIIFGSM are 0.807 for the first case, which is the same with TIMIFGSM and followed by 0.686 of IFGSM as well as MIFGSM, while our BEF achieves the best value of 0.958. Our CBEF result generated from this case gets a SSIM value of only 0.668. But, for the fourth case, our CBEF obtains the SSIM value of 0.76, which is better than the best baseline result 0.736 of

| Crafted from   | ResNet50  |              |          | MobileNet |              |           | EfficientNet |           |              |
|----------------|-----------|--------------|----------|-----------|--------------|-----------|--------------|-----------|--------------|
| Attacked model | MobileNet | EfficientNet | ResNet50 | ResNet50  | EfficientNet | MobileNet | ResNet50     | MobileNet | EfficientNet |
| FGSM           | 13.6      | 14.8         | 11.0     | 7.7       | 11.7         | 10.7      | 7.5          | 10.2      | 13.9         |
| TIFGSM         | 13.7      | 14.7         | 11.0     | 7.7       | 11.7         | 10.5      | 7.4          | 10.3      | 20.2         |
| IFGSM          | 14.3      | 15.2         | 100      | 47.4      | 21.6         | 100       | 54.7         | 21.9      | 100          |
| TIIFGSM        | 62.9      | 18.9         | 100      | 15.8      | 14.1         | 100       | 14.4         | 32.2      | 100          |
| MIFGSM         | 14.0      | 15.0         | 100      | 18.3      | 21.5         | 100       | 26.6         | 16.8      | 100          |
| TIMIFGSM       | 57.8      | 20.9         | 100      | 13.6      | 15.5         | 100       | 12.6         | 24.4      | 100          |
| BEF (ours)     | 9.5       | 10.9         | 98.6     | 7.8       | 8.1          | 99.7      | 9.1          | 8.7       | 98.1         |
| CBEF (ours)    | 84.6      | 81.8         | 99.6     | 37.0      | 82.9         | 100       | 24.9         | 47.1      | 99.6         |

Table 1: Adversarial comparison results on EyePACS dataset. It contains the success rates (%) of transfer & whitebox adversarial attacks among three fine-tuned models: ResNet50, MobileNet, and EfficientNet, using six baseline methods with maximum perturbation of 32 and two versions of our method, *i.e.*, BEF and CBEF. For each three columns, the whitebox attack results are shown in the last one. The first and second columns exhibit the transfer attack results. We highlight the top three results with red, yellow, and green, respectively.

TIIFGSM. Considering the BRISQUE, TIIFGSM and TIMIFGSM are both 37.39 for the last case, which are the best among all baselines, while our BEF and CBEF get 12.9 and 25.94, respectively. The visualization results show that our CBEF method tends to mislead the DNN model with over exposure operation, which takes major responsibility for the weakness of our method in terms of SSIM metric. Nevertheless, due to the Laplacian pyramid fusion process in our framework, our results have rarely noise-like patterns in our adversarial results, which commonly occurs in the additive-perturbation-based baselines. The noise-free outputs finally bring us the best (*i.e.*, lowest) BRISQUE values. Moreover, the over exposure pattern of the CBEF results with respect to attack task indicates that DR grading is sensitive to exposure change and lower contrast.

### 4.3 Ablation study

In this section, we first test the success rate of transfer attack, *i.e.*, transferability, of BEF and CBEF. Then, we further study the influence of multiple hyper-parameters introduced in Sec. 3 on our transferability, including the level  $L$  of Laplacian pyramid space in adversarial bracketed exposure fusion as well as the kernel size  $K$  in convolutional bracketed exposure fusion.

**Comparison on Transferability.** Transferability refers to the attack capability of adversary in attacking one target model with the adversarial examples crafted from another model. It is important to evaluate the transferability as it indicates the potential ability in realizing effective blackbox attack which is more consistent with the attack problem in physical world. For fair comparison, we conduct the transferability experiment with the adversarial examples having similar image quality. Considering the performance of both SSIM and BRISQUE for all baselines and our methods in Fig. 3, we finally choose 32 for all additive-perturbation-based baselines and 0.01 for step size in our methods.

We first craft adversarial examples from the three models, *e.g.*, ResNet50, MobileNet and EfficientNet, respectively, and feed them to each model for evaluation. At last, we get nine attack success rates for each attack method including three whitebox attacks and six transfer attacks. Table 1 shows the results. Generally, we draw a similar conclusion

that most baselines as well as our methods, *i.e.*, BEF and CBEF, achieve almost 100% success rate when they implement whitebox attack. Besides, we have following observations in terms of transferability: ❶ Although BEF shows a significant advantage in image quality, its transferability is lower than most baselines. Considering the adversarial example crafted from MobileNet, the whitebox attack of BEF and CBEF achieve similar success rates of 99.7% and 100%. However, the transfer attack to ResNet50 and EfficientNet by BEF only has success rates of 7.8% and 8.1%, even lower than FGSM and TIFGSM. ❷ CBEF sacrifices image quality comparing with BEF, exchanging strong transferability. The transfer attack against to EfficientNet by CBEF using adversarial examples crafted from MobileNet has a success rate of 82.9%, which is the best among all methods. And the transfer attack success rate for ResNet50 is 37%, lying on the second place which follows 47.4% of IFGSM. We can find similar results on other two models.

**Effects of the number of pyramid level  $L$ .** As mentioned in Sec. 3, we introduce the Laplacian-pyramid space to overcome the noise pattern generated by simple fusion of Eq. 1. Here, we tune the pyramid level  $L$  in Eq. 4 and Eq. 7 to check its influence on the attack success rate of BEF and CBEF. Specifically, we set  $L = 1, 3, 5$  in this experiment and generate three different versions for BEF and CBEF, respectively. Note that,  $L = 1$  refers to no pyramid fusion process is applied. The results are shown in Table. 2.

First, the whitebox attacks under BEF and CBEF are affected by the increase of  $L$ . Taking ResNet50 as an example, the whitebox attack success rates of BEF and CBEF with no pyramid ( $L = 1$ ) are 100%. However, as  $L$  increases, the success rates drop to 94.6% and 98.9%, respectively. Second, the success rate of transfer attack of BEF is heavily affected by  $L$ . For example, when we conduct the transfer attack to MobileNet and EfficientNet with the adversarial examples crafted from ResNet50, BEF has the success rates of 45.2% and 45.7% with  $L = 1$ . However, when we introduce pyramid fusion and set  $L = 3$ , the transfer attack success rates of BEF decrease to 9.5% and 10.9%. Moreover, as we increase  $L$  to 5, the success rates keep dropping to 8.6% and 10.7%.

| Crafted from     | ResNet50  |              |          | MobileNet |              |           | EfficientNet |           |              |
|------------------|-----------|--------------|----------|-----------|--------------|-----------|--------------|-----------|--------------|
| Attacked model   | MobileNet | EfficientNet | ResNet50 | ResNet50  | EfficientNet | MobileNet | ResNet50     | MobileNet | EfficientNet |
| BEF ( $L = 1$ )  | 45.2      | 45.7         | 100      | 46.2      | 65.7         | 100       | 64           | 80.9      | 100          |
| BEF ( $L = 3$ )  | 9.5       | 10.9         | 98.6     | 7.8       | 8.1          | 99.7      | 9.1          | 8.7       | 98.1         |
| BEF ( $L = 5$ )  | 8.6       | 10.7         | 94.6     | 7.7       | 7.4          | 96.2      | 7.7          | 6.6       | 84.2         |
| CBEF ( $L = 1$ ) | 31.2      | 29.3         | 100      | 33.8      | 33.1         | 100       | 56.7         | 76.3      | 100          |
| CBEF ( $L = 3$ ) | 84.6      | 81.8         | 99.6     | 37.0      | 82.9         | 100       | 24.9         | 47.1      | 99.6         |
| CBEF ( $L = 5$ ) | 25.2      | 29.7         | 98.9     | 38.6      | 59.7         | 98.0      | 50.3         | 28.3      | 88.9         |

Table 2: Adversarial comparison results on EyePACS dataset. It contains the success rates (%) of transfer & whitebox adversarial attacks on three fine-tuned models: ResNet50, MobileNet, and EfficientNet, using our methods, *i.e.*, BEF and CBEF, with different number of Laplacian-pyramid level ( $L = 1, 3, 5$ ). For each three columns, the whitebox attack results are shown in the last one. The first and second columns exhibit the transfer attack results.

| Crafted from | ResNet50  |              |          | MobileNet |              |           | EfficientNet |           |              |
|--------------|-----------|--------------|----------|-----------|--------------|-----------|--------------|-----------|--------------|
| ( $L, K$ )   | MobileNet | EfficientNet | ResNet50 | ResNet50  | EfficientNet | MobileNet | ResNet50     | MobileNet | EfficientNet |
| (1, 1)       | 45.2      | 45.7         | 100      | 46.2      | 65.7         | 100       | 64           | 80.9      | 100          |
| (1, 3)       | 31.2      | 29.3         | 100      | 33.8      | 33.1         | 100       | 56.7         | 76.3      | 100          |
| (1, 5)       | 30.6      | 27.5         | 100      | 39.4      | 32.5         | 100       | 61.5         | 71.2      | 100          |
| (3, 1)       | 9.5       | 10.9         | 98.6     | 7.8       | 8.1          | 99.7      | 9.1          | 8.7       | 98.1         |
| (3, 3)       | 84.6      | 81.8         | 99.6     | 37.0      | 82.9         | 100       | 24.9         | 47.1      | 99.6         |
| (3, 5)       | 36.5      | 37.3         | 94.9     | 28.4      | 62.2         | 99.9      | 15.7         | 32.0      | 99.8         |

Table 3: Adversarial comparison results on EyePACS dataset. It contains the success rates (%) of transfer & whitebox adversarial attacks among three fine-tuned models: ResNet50, MobileNet, and EfficientNet, using our method with different settings of pyramid level ( $L = 1, 3$ ) and kernel sizes ( $K = 1, 3, 5$ ). For each three columns, the whitebox attack results are shown in the last one. The first and second columns exhibit the transfer attack results.

Above two observations indicate the negative effect of pyramid fusion for the success rate of attack. It brings benefit for image quality and damage for attack capability in the meantime. In contrast, the CBEF conquers this trend by extending the element-wise weight to the convolution kernel. More specifically, the CBEF, with pyramid fusion level  $L = 3$ , achieves the transfer attack success rates of 84.6% and 81.8% when it attacks MobileNet and EfficientNet using adversarial examples crafted from ResNet50. These are higher than that results of setting  $L = 1$ . Such results hint that convolution-based attack benefits the high success rate of transfer attack. However, we also observe that when  $L = 1$  the CBEF has lower success rate than BEF. We argue that this phenomenon is directly related to the kernel size for CBEF. Please find detailed explanation in the following.

**Effects of the kernel size  $K$ .** We have show the advantages of convolutional bracketed exposure fusion in improving the transferability. Here, we further conduct an experiment to study the influence of kernel size  $K$  in Eq. 7 on the transferability of CBEF under different pyramid settings. More specifically, we pick two pyramid fusion level, *i.e.*,  $L = 1, 3$ , and tune the kernel size  $K = 1, 3, 5$  in our experiment. The results are shown in Table. 3.

It can be seen that, when  $L = 1$ , transfer attack success rate drops with the increase of kernel size. However, when  $L = 3$ , the success rate of transfer attack increase with the  $K$  from 1 to 3 and drop again with  $K$  from 3 to 5. Considering the same kernel size, *e.g.*,  $K = 3$ , the success rates of transfer attack increase significantly. We have similar results

when  $K = 5$ . However, when  $K = 1$ , *i.e.*, the CBEF is degraded to BEF, the attack success rate reduces significantly.

Overall, both kernel size  $K$  and number of the pyramid level affect the success rate of transfer attack significantly.

## 5 Conclusion

We proposed a novel adversarial attack method, *i.e.*, *adversarial exposure attack*, to show the potential threat of camera exposure to automated DNN-based diabetic retinopathy (DR) diagnostic system. We first demonstrated challenges of this new task through a straightforward method, *i.e.*, *multiplicative-perturbation-based exposure attack*, where the naturalness of the exposure, *i.e.*, inherent smooth property, cannot be maintained. Then, we proposed the *adversarial bracketed exposure fusion* based attack in which the attack is formulated as the fusion problem of bracketed exposure sequence. The element-wise multiplicative fusion weight maps can be tuned to generate realistic adversarial exposure examples. Moreover, we further proposed an enhanced version by extending the multiplicative fusion to the convolution operation that helps achieve significantly high success rate of the transfer attack. We have validated our method on a real and popular DR detection dataset, demonstrating that our method can generate high image quality of adversarial examples and high success rate of the transfer attack. We think this work would help develop exposure-robustness DNN-based automated DR diagnostic system. This paper explored the exposure attack for classification. However, its influence on other tasks, *e.g.*, visual object

tracking (Guo et al. 2020c,a, 2017a,b; Zhou et al. 2017), natural image classification (Guo et al. 2020b), face recognition (Wang et al. 2020c), etc., are also worthy of study. Moreover, we plan to investigate the interplay of exposure attack with other attack models (Cheng et al. 2020; Chan et al. 2018; Sun et al. 2020; Zhai et al. 2020) as well as the studies (Huang et al. 2020c; Wang et al. 2020b; Qi et al. 2020; Huang et al. 2020b,a; Wang et al. 2020a) related to the DeepFake problems.

## References

- Akram, M. U.; Khalid, S.; Tariq, A.; Khan, S. A.; and Azam, F. 2014. Detection and classification of retinal lesions for grading of diabetic retinopathy. *Computers in biology and medicine* 45: 161–171.
- Baluja, S.; and Fischer, I. 2017. Adversarial transformation networks: Learning to generate adversarial examples. *arXiv preprint arXiv:1703.09387*.
- Carlini, N.; and Wagner, D. 2017. Towards evaluating the robustness of neural networks. In *2017 IEEE Symposium on Security and Privacy (SP)*, 39–57. IEEE.
- Chan, A.; Ma, L.; Juefei-Xu, F.; Xie, X.; Liu, Y.; and Ong, Y. S. 2018. Metamorphic relation based adversarial attacks on differentiable neural computer. *arXiv preprint arXiv:1809.02444*.
- Chen, P.-Y.; Zhang, H.; Sharma, Y.; Yi, J.; and Hsieh, C.-J. 2017. Zoo: Zeroth order optimization based black-box attacks to deep neural networks without training substitute models. In *Proceedings of the 10th ACM Workshop on Artificial Intelligence and Security*, 15–26.
- Cheng, Y.; Guo, Q.; Juefei-Xu, F.; Xie, X.; Lin, S.-W.; Lin, W.; Feng, W.; and Liu, Y. 2020. Pasadena: Perceptually Aware and Stealthy Adversarial Denoise Attack. *arXiv preprint arXiv:2007.07097*.
- Dong, Y.; Liao, F.; Pang, T.; Su, H.; Zhu, J.; Hu, X.; and Li, J. 2018. Boosting adversarial attacks with momentum. In *Proceedings of the IEEE conference on computer vision and pattern recognition*, 9185–9193.
- Dong, Y.; Pang, T.; Su, H.; and Zhu, J. 2019. Evading defenses to transferable adversarial examples by translation-invariant attacks. In *Proceedings of the IEEE Conference on Computer Vision and Pattern Recognition*, 4312–4321.
- Gargeya, R.; and Leng, T. 2017. Automated identification of diabetic retinopathy using deep learning. *Ophthalmology* 124(7): 962–969.
- Goodfellow, I. J.; Shlens, J.; and Szegedy, C. 2014. Explaining and harnessing adversarial examples. *arXiv preprint arXiv:1412.6572*.
- Gulshan, V.; Peng, L.; Coram, M.; Stumpe, M. C.; Wu, D.; Narayanaswamy, A.; Venugopalan, S.; Widner, K.; Madams, T.; Cuadros, J.; et al. 2016. Development and validation of a deep learning algorithm for detection of diabetic retinopathy in retinal fundus photographs. *Jama* 316(22): 2402–2410.
- Guo, C.; Gardner, J. R.; You, Y.; Wilson, A. G.; and Weinberger, K. Q. 2019. Simple black-box adversarial attacks. *arXiv preprint arXiv:1905.07121*.
- Guo, Q.; Feng, W.; Zhou, C.; Huang, R.; Wan, L.; and Wang, S. 2017a. Learning dynamic siamese network for visual object tracking. In *Proceedings of the IEEE international conference on computer vision*, 1763–1771.
- Guo, Q.; Feng, W.; Zhou, C.; Pun, C.-M.; and Wu, B. 2017b. Structure-regularized compressive tracking with online data-driven sampling. *IEEE Transactions on Image Processing* 26(12): 5692–5705.
- Guo, Q.; Han, R.; Feng, W.; Chen, Z.; and Wan, L. 2020a. Selective spatial regularization by reinforcement learned decision making for object tracking. *IEEE Transactions on Image Processing* 29: 2999–3013.
- Guo, Q.; Juefei-Xu, F.; Xie, X.; Ma, L.; Wang, J.; Feng, W.; and Liu, Y. 2020b. ABBA: Saliency-Regularized Motion-Based Adversarial Blur Attack. *arXiv preprint arXiv:2002.03500*.
- Guo, Q.; Xie, X.; Juefei-Xu, F.; Ma, L.; Li, Z.; Xue, W.; Feng, W.; and Liu, Y. 2020c. SPARK: Spatial-aware online incremental attack against visual tracking. In *Proceedings of the European Conference on Computer Vision (ECCV)*.
- Hayes, J.; and Danezis, G. 2017. Machine learning as an adversarial service: Learning black-box adversarial examples. *arXiv preprint arXiv:1708.05207* 2.
- He, K.; Gkioxari, G.; Dollár, P.; and Girshick, R. 2017. Mask r-cnn. In *Proceedings of the IEEE international conference on computer vision*, 2961–2969.
- He, K.; Zhang, X.; Ren, S.; and Sun, J. 2016. Deep residual learning for image recognition. In *Proceedings of the IEEE conference on computer vision and pattern recognition*, 770–778.
- Howard, A. G.; Zhu, M.; Chen, B.; Kalenichenko, D.; Wang, W.; Weyand, T.; Andreetto, M.; and Adam, H. 2017. Mobilenets: Efficient convolutional neural networks for mobile vision applications. *arXiv preprint arXiv:1704.04861*.
- Huang, Y.; Juefei-Xu, F.; Guo, Q.; Xie, X.; Ma, L.; Miao, W.; Liu, Y.; and Pu, G. 2020a. FakeRetouch: Evading DeepFakes Detection via the Guidance of Deliberate Noise. *arXiv preprint arXiv*.
- Huang, Y.; Juefei-Xu, F.; Wang, R.; Guo, Q.; Ma, L.; Xie, X.; Li, J.; Miao, W.; Liu, Y.; and Pu, G. 2020b. FakePolisher: Making DeepFakes More Detection-Evasive by Shallow Reconstruction. *arXiv preprint arXiv:2006.07533*.
- Huang, Y.; Juefei-Xu, F.; Wang, R.; Xie, X.; Ma, L.; Li, J.; Miao, W.; Liu, Y.; and Pu, G. 2020c. FakeLocator: Robust Localization of GAN-Based Face Manipulations via Semantic Segmentation Networks with Bells and Whistles. *arXiv preprint arXiv:2001.09598*.
- Krause, J.; Gulshan, V.; Rahimy, E.; Karth, P.; Widner, K.; Corrado, G. S.; Peng, L.; and Webster, D. R. 2018. Grader variability and the importance of reference standards for evaluating machine learning models for diabetic retinopathy. *Ophthalmology* 125(8): 1264–1272.
- Kumar, N.; Rajwade, A. V.; Chandran, S.; and Awate, S. P. 2017. Kernel generalized-Gaussian mixture model for robust abnormality detection. In *International Conference on Medical Image Computing and Computer-Assisted Intervention*, 21–29. Springer.
- Kurakin, A.; Goodfellow, I.; and Bengio, S. 2016. Adversarial examples in the physical world. *arXiv preprint arXiv:1607.02533*.
- Lee, R.; Wong, T. Y.; and Sabanayagam, C. 2015a. *Diabetic Retinopathy Detection*. URL <https://www.kaggle.com/c/diabetic-retinopathy-detection>.
- Lee, R.; Wong, T. Y.; and Sabanayagam, C. 2015b. Epidemiology of diabetic retinopathy, diabetic macular edema and related vision loss. *Eye and vision* 2(1): 1–25.

- Li, X.; Hu, X.; Yu, L.; Zhu, L.; Fu, C.-W.; and Heng, P.-A. 2019. CANet: Cross-Disease Attention Network for Joint Diabetic Retinopathy and Diabetic Macular Edema Grading. *IEEE transactions on medical imaging* 39(5): 1483–1493.
- Mansour, R. F. 2018. Deep-learning-based automatic computer-aided diagnosis system for diabetic retinopathy. *Biomedical engineering letters* 8(1): 41–57.
- Mertens, T.; Kautz, J.; and Van Reeth, F. 2009. Exposure fusion: A simple and practical alternative to high dynamic range photography. In *Computer graphics forum*, volume 28, 161–171. Wiley Online Library.
- Mittal, A.; Moorthy, A. K.; and Bovik, A. C. 2012. No-reference image quality assessment in the spatial domain. *IEEE Transactions on image processing* 21(12): 4695–4708.
- Moosavi-Dezfooli, S.-M.; Fawzi, A.; and Frossard, P. 2016. Deep-fool: a simple and accurate method to fool deep neural networks. In *CVPR*, 2574–2582.
- Papernot, N.; McDaniel, P.; Jha, S.; Fredrikson, M.; Celik, Z. B.; and Swami, A. 2016. The limitations of deep learning in adversarial settings. In *2016 IEEE European symposium on security and privacy (EuroS&P)*, 372–387. IEEE.
- Qi, H.; Guo, Q.; Juefei-Xu, F.; Xie, X.; Ma, L.; Feng, W.; Liu, Y.; and Zhao, J. 2020. DeepRhythm: Exposing DeepFakes with Attentional Visual Heartbeat Rhythms. *arXiv preprint arXiv:2006.07634* .
- Shen, Z.; Fu, H.; Shen, J.; and Shao, L. 2020. Understanding and Correcting Low-quality Retinal Fundus Images for Clinical Analysis. *arXiv preprint arXiv:2005.05594* .
- Silberman, N.; Ahrlich, K.; Fergus, R.; and Subramanian, L. 2010. Case for Automated Detection of Diabetic Retinopathy. In *AAAI Spring Symposium: Artificial Intelligence for Development*.
- Su, J.; Vargas, D. V.; and Sakurai, K. 2019. One pixel attack for fooling deep neural networks. *IEEE Transactions on Evolutionary Computation* .
- Sun, J.; Zhang, T.; Xie, X.; Ma, L.; Zheng, Y.; Chen, K.; and Liu, Y. 2020. Stealthy and efficient adversarial attacks against deep reinforcement learning. *arXiv preprint arXiv:2005.07099* .
- Szegedy, C.; Zaremba, W.; Sutskever, I.; Bruna, J.; Erhan, D.; Goodfellow, I.; and Fergus, R. 2013. Intriguing properties of neural networks. *arXiv preprint arXiv:1312.6199* .
- Tan, M.; and Le, Q. V. 2019. Efficientnet: Rethinking model scaling for convolutional neural networks. *arXiv preprint arXiv:1905.11946* .
- Wang, R.; Juefei-Xu, F.; Guo, Q.; Huang, Y.; Xie, X.; Ma, L.; Liu, Y.; and Wang, L. 2020a. DeepTag: Robust Image Tagging for DeepFake Provenance. *arXiv preprint arXiv* .
- Wang, R.; Juefei-Xu, F.; Huang, Y.; Guo, Q.; Xie, X.; Ma, L.; and Liu, Y. 2020b. DeepSonar: Towards Effective and Robust Detection of AI-Synthesized Fake Voices. *arXiv preprint arXiv:2005.13770* .
- Wang, R.; Juefei-Xu, F.; Xie, X.; Ma, L.; Huang, Y.; and Liu, Y. 2019. Amora: Black-box adversarial morphing attack. *arXiv preprint arXiv:1912.03829* .
- Wang, R.; Juefei-Xu, F.; Xie, X.; Ma, L.; Huang, Y.; and Liu, Y. 2020c. Amora: Black-box adversarial morphing attack. In *ACM Multimedia Conference (ACMMM)*.
- Wang, Z.; Bovik, A. C.; Sheikh, H. R.; and Simoncelli, E. P. 2004. Image quality assessment: from error visibility to structural similarity. *IEEE transactions on image processing* 13(4): 600–612.
- Yang, Y.; Li, T.; Li, W.; Wu, H.; Fan, W.; and Zhang, W. 2017. Lesion detection and grading of diabetic retinopathy via two-stages deep convolutional neural networks. In *International Conference on Medical Image Computing and Computer-Assisted Intervention*, 533–540. Springer.
- Zhai, L.; Juefei-Xu, F.; Guo, Q.; Xie, X.; Ma, L.; Feng, W.; Qin, S.; and Liu, Y. 2020. It’s Raining Cats or Dogs? Adversarial Rain Attack on DNN Perception. *arXiv preprint arXiv* .
- Zhou, C.; Guo, Q.; Wan, L.; and Feng, W. 2017. Selective object and context tracking. In *2017 IEEE International Conference on Acoustics, Speech and Signal Processing (ICASSP), 1947–1951*. IEEE.
- Zhou, Y.; He, X.; Huang, L.; Liu, L.; Zhu, F.; Cui, S.; and Shao, L. 2019. Collaborative learning of semi-supervised segmentation and classification for medical images. In *Proceedings of the IEEE Conference on Computer Vision and Pattern Recognition, 2019–2088*.